Electromagnetic Radiation Force of Vortex Electromagnetic wave exerted on a perfect electromagnetic conductor (PEMC) Sphere

Muhammad Arfan[1], Abdul Ghaffar[1,*], Majeed. A. S. Alkanhal[2], Yasin Khan[2], Ali. H. Alqahtani[3], Sajjad Ur Rehman[4]

[1] *Dept. of Physics, University of Agriculture, Faisalabad 38000, Pakistan*

[2] *Dept. of Electrical Engineering, King Saud University, Riyadh, Saudi Arabia*

[3] *Dept. of Electrical Engineering, College of Applied Engineering, King Saud University, Al-Muzahimiyah Branch, Saudi Arabia*

[4] *Dept. of Electrical Engineering, Namal College, Mianwali, Pakistan*

**Corresponding author: aghaffar16@uaf.edu.pk*

Abstract

In this manuscript, the electromagnetic (EM) radiation force (RF) exerted on a perfect electromagnetic conductor (PEMC) sphere by a vortex electromagnetic (VEM) wave with spiral phase distribution had been investigated. The analytical formulation of EM fields is being done in the framework of Mie theory, while the field expressions are being modeled considering the features of VEM wave for PEMC sphere. Initially, the incident field coefficients are evaluated using definite integrals. The scattering coefficients are then determined by imposing boundary conditions at the surface of PEMC sphere i.e., at $r = a$, leading to a linear system of equations computed via solving matrix. So, a lengthy calculation yields undetermined scattered field coefficients relative to incident field coefficients. The cross-section (Q) factors i.e., scattering (Q_{sca}) and extinction (Q_{ext}) have been computed. The influence of sphere size parameter (ρ) and beam waist radius (w_0) versus scattering angle (α°) for the RF along with Q_{sca} has been numerically analyzed. As no loss of energy occurs inside PEMC sphere so absorption $((Q_{abs}) = 0)$, by virtue of the energy conservation principle then, $Q_{ext} = Q_{sca}$. Under specific condition, we implemented present results on Q_{sca} towards light without orbital angular momentum (OAM) i.e., $(l = 0)$ and plane wave for the PEMC sphere. The research work has potential applications towards particle manipulation, optical technology, and optical tweezers.

Keywords: Field modes; OAM; PEMC sphere; radiation force; scattering; VEM wave.

1. Introduction

Electromagnetic (EM) waves with OAM have gotten a lot of interest and research due to their efficiency in compelling communications and remarkable future applications (Long *et al.*, 2018; Yao *et al.*, 2019; Liu *et al.*, 2018). The concept of OAM has been suggested for the first time in 1992, and it has never been employed in a real application before that (Allen *et al.*, 1992). Since then, OAM waves have sparked a lot of attention in the field of light and optics (Barnett and Allen, 1994; Gibson *et al.*, 2004). The key features of OAM are not only limited to the material characterization and light manipulation (Thakur and Berakdar, 2012) but also valid for image

forming systems, topological charge, optical tweezers, quantum optics, ultra-fast communications, and holography (Yao and Padgett, 2011; Padgett, 2014; Thidé *et al.*, 2007).

The shifting of OAM of the twisting-shaped beams rotates the objects (Molina-Terriza *et al.*, 2007). The helicity produced in the VEM wave owes to the azimuthal mode. The helical profile structure can be understood as a signature of discrete OAM. On interacting with material particles these show unusual EM response (O'neil *et al.*, 2002). Since the introduction of OAM waves in radio wireless communications in 2007, research in this area has been increasingly focused (Thidé *et al.*, 2007).

Unlike plane EM wave propagation (Shahid *et al.*, 2021), VEM wave associates with the characteristics of a coherent light beam with a dependency factor of $e^{il\varphi}$, in which l is the OAM mode number/topological charge and φ is the azimuthal angle. It ranges from zero to infinite. Due to this parameter, the doughnut shape radiation pattern of a light beam exists. The helical wave front feature of VEM wave that illuminates a target can alter the scattering effect.

In 1873, the concept of electromagnetic radiation force (RF) was introduced (Achard, 2005). Later on, it was realized that all the mechanical effects were induced due to this RF exerted on the particle (Nichols and Hull, 1903; Lebedev, 1883). On interacting the radiation with matter, an exchange of momentum takes place. The momentum can have both angular as well as linear contributions. Polarization gives the angular part of the momentum and spatial distribution gives the orbital part of the momentum. So, EM waves have fundamental property known as OAM. In principally, OAM is considered as a beam associated with manifold number of OAM modes which may have integer or non-integer values (Cheng *et al.*, 2018). The OAM is also capable to rotate the particles about the propagation axis.

The study of RF has been studied by (Mitri, 2019a) on PEMC circular cylinder; He showed that the interaction of optical wave with a medium permitting rotary polarization i.e., circular cylinder produces coupled polarized internal as well as dispersed fields. The analytical and numerical study of RF involves the interaction of the plane EM wave with different material arrangement i.e., rigid bodies in a sound field (Olsen *et al.*, 1958), electrically conducting cylindrical particles (Mitri, 2018), PEMC sphere (Mitri *et al.*, 2020), cylinder exhibiting rotatory polarization (Mitri, 2019c), optical line source on a cylinder material (Mitri, 2019b), and elliptical-shaped cylinder (Mitri, 2016).

The most common scenario is research papers on RF computation for Gaussian beams in the available literature. As a result, several researchers have focused on the precise computation of RF using the Maxwell equations for Gaussian beams (Li et al., 2011; Azarpeyvand and Azarpeyvand, 2013; Kim and Kim, 2006; Kotlyar and Nalimov, 2006). Kim *et al.* (Kim and Lee, 1983) calculated the radiation pressure exerted on the sphere. The incident laser beam field expressions are attained by using the Complex Source Point Method (CSPM) to calculate the light field distributions.

As a result, research into the scattering and propagation characteristics of Laguerre–Gaussian (LG) vortex beam is critical in understanding how energy and OAM are transferred from light to trapped particles (Simpson *et al.*, 1996; O'neil *et al.*, 2002). The study of RF in the OAM domain has also been conducted by many researchers. Qu *et al.* (Qu *et al.*, 2015) analyzed the RF of an

LG beam exerted on a uniaxial anisotropic sphere comprehensively. The CSPM is used to expand the LG vortex beam in terms of Spherical vector wave function (SVWF's). So, numerical study of RF became feasible. In addition, the interaction of LG beam with particles for various shapes has been studied by Qu *et al.* (Qu *et al.*, 2016a; Qu *et al.*, 2018; Qu *et al.*, 2016b; Qu *et al.*, 2015) extensively. Yu *et al.* (Yu and She, 2015) investigated the RF imposed by focused LG beams on a sphere.

Li *et al.* (Li *et al.*, 2021) demonstrated that the focused LG beam exerts a negative torque on the particle, which is equivalent to the optical pulling force. So, keeping the LG beam strongly focused, the particle rotation and the beam with OAM might be in the opposite direction. They added a new thinking to the existing research. Kiselev *et al.* (Kiselev and Plutenko, 2016) studied the far-field equations for the optical (radiation) force exerted on a spherical (Mie) particle by LG light beams.

Simpson *et al.* (Simpson *et al.*, 1996) investigated the optical manipulation of the LG beam. They modeled the axial trapping forces inside optical tweezers stemming from LG laser modes. Arfan et al. (Arfan *et al.*, 2022a; Arfan *et al.*, 2021) studied the LG beam scattering from a chiral-coated PEMC cylinder and a simple PEMC cylinder. Changing beam modes, the scattering field distribution changes. However, to the best of author's knowledge, the study of optical RF for LG VEM wave towards PEMC sphere has not been described in literature.

So, in this paper, the analytical expressions of VEM wave in terms of SVWF's are attained and employed to investigate the RF on a PEMC sphere. On expanding plane wave using SVWF's, VEM wave is expressed with reference to SVWF's on the basis of the relationship between plane wave ($l = 0$) and VEM wave ($l = 1$) (Arfan *et al.*, 2022b). Then the expressions regarding RF for the OAM wave are derived. Lastly, the influence of different parameters as, w_0, ρ, and $M\eta_0$ for the Q_{sca} and RF have been studied.

The layout of the paper is organized as follows. The generalized Lorenz-Mie theory for PEMC sphere and SVWF's is given in Section 2. Theoretical model of VEM wave in terms of SVWF's is expressed in Section 3. In Section 4, optical RF for the VEM wave exerted on the PEMC sphere is described. In Section 5, cross-section (Q) factors for VEM wave towards the PEMC sphere are calculated. Section 6 is dedicated to check the numerical validity of our research work. Section 7 presents the numerical analysis of the results, along with discussion. The conclusion is mapped out in section 8.

2. Generalized Lorenz-Mie Theory for PEMC Sphere

Metamaterials are artificial (man-made) structures designed to achieve characteristics not available in nature (Lapine and Tretyakov, 2007). The response of a metamaterial to an incident EM wave can be characterized by effective permittivity and effective permeability (Wartak *et al.*, 2011). One such type of material with excellent properties is called PEMC (Sihvola, 2007). EM fields cannot propagate in this medium. On substituting the admittance parameter ($M = 0, \infty$) for PEMC, the perfect magnetic conductor (PMC) as well as perfect electric conductor (PEC) media can be realized as special cases of the PEMC medium. For ($0 < M < \infty$), PEMC holds a boundary with

nonreciprocal aspects (Capolino, 2017). The focal point of the PEMC medium; it acts as a boundary to rotate the plane of polarization of the reflected EM wave, which can find amazing applications in the antenna and microwave domain (Sihvola and Lindell, 2017).

The SVWF's are introduced in order to solve Maxwell's equations in spherical polar coordinates. In terms of spherical coordinate system (r, θ, φ), these are given as

$$\vec{M}_{\sigma mn}^{(l)} = \vec{\nabla} \times [\vec{r} Y_{\sigma mn}(\theta, \varphi) z_n^l(kr)] \tag{1}$$

$$\vec{N}_{\sigma mn}^{(l)} = \frac{1}{k} [\vec{\nabla} \times \vec{M}_{\sigma mn}^{(l)}] \tag{2}$$

where $Y_{\sigma mn}(\theta, \varphi)$ represents spherical harmonic. Parity of spherical harmonics is denoted by σ which may be even or odd depending on $\sigma = e$ or $\sigma = o$. The radial function $z_n^l(kr)$ represents three different kinds of special functions as Spherical Bessel $j_n(kr)$, Spherical Neumann $n_n(kr)$, and Spherical Hankel $h_n(kr)$ as $n = 1,2,3$ respectively. SVWF's are given as

$$\vec{M}_{emn} = [-\pi_n^m(\theta)\, Sin\,(m\phi)\, \hat{e_\theta} - \tau_n^m(\theta)\, Cos\,(m\phi)\, \hat{e_\phi}\,]\, z_n(\rho) \tag{3}$$

$$\vec{M}_{omn} = [\pi_n^m(\theta)\, Cos\,(m\phi)\ \hat{e_\theta} - \tau_n^m(\theta)\ Sin\,(m\phi)\, \hat{e_\phi}\ ]\, z_n(\rho) \tag{4}$$

$$\vec{N}_{emn} = \frac{n(n+1)\, z_n(\rho)}{\rho} Cos\,(m\phi) \hat{e_r} + [\tau_n^m(\theta)\, Cos\,(m\phi)\, \hat{e_\theta} - \pi_n^m(\theta)\, Sin\,(m\phi)\ \hat{e_\phi}] \frac{d}{d\boldsymbol{\rho}} (\rho z_n(\rho))\ ) \tag{5}$$

$$\vec{N}_{omn} = \frac{n(n+1)\, z_n(\rho)}{\rho}\ Sin\,(m\phi)\, \hat{e_r} + [\tau_n^m(\theta)\, Sin\,(m\phi)\, \hat{e_\theta} + \pi_n^m(\theta)\, Cos\,(m\phi)\ \hat{e_\phi}] \frac{d}{d\boldsymbol{\rho}} (\rho z_n(\rho)) \tag{6}$$

$\pi_n^m(\theta)$ and $\tau_n^m(\theta)$ are the angle-dependent functions defined as

$$\pi_n^m(\theta) = \frac{m\, P_n^m(Cos\theta)}{Sin\theta} \tag{7}$$

$$\tau_n^m(\theta) = \frac{d}{d\theta} P_n^m(Cos\theta) \tag{8}$$

$P_n^m(Cos\theta)$ be the associated Legendre Polynomial. The incident field is expressed using spherical Bessel function $J_n(.)$ while, scattered field is designated by the spherical Hankel function $h_n(.)$. Here, $\hat{e_r}$, $\hat{e_\theta}$, and $\hat{e_\phi}$ are the unit vectors of the spherical polar coordinates system. The equations (3)-(8) are employed for different field modes associated with the VEM wave towards PEMC sphere.

3. Theoretical Model of VEM wave in SVWF's

We consider a PEMC sphere with radius a that is illuminated by a linearly polarized LG beam with angular frequency ω and helical wave front factor $e^{il\varphi}$ as shown in Figure 1.

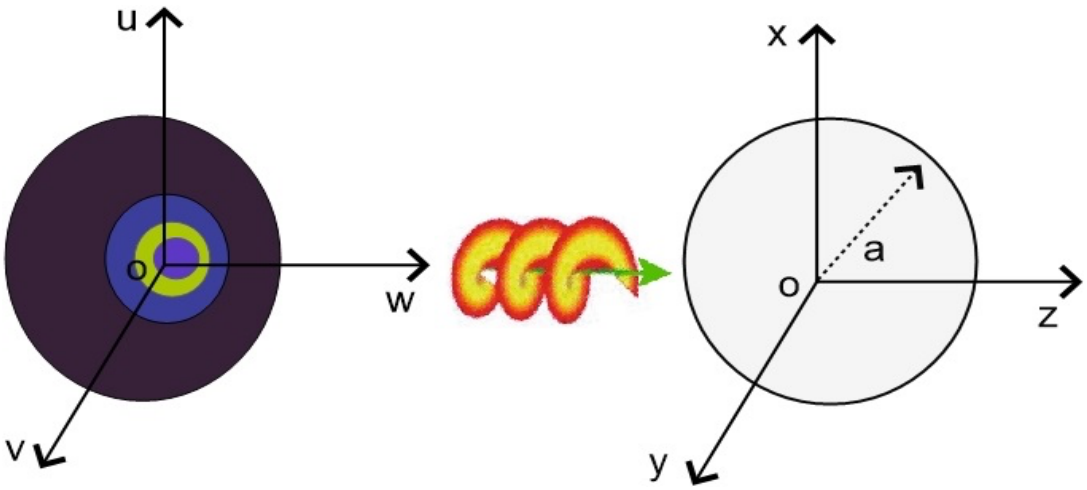

Fig. 1. A PEMC sphere with radius a illuminated by an LG_{01} beam.

For an LG VEM wave, the incident electric field with suppressing $e^{-i\omega t}$ time dependency factor is given by,

$$\vec{E}^{inc}(\rho_t, \varphi, z) = E_0 \left(\frac{\rho_t \sqrt{2}}{w_0}\right)^l L_p^l\left(\frac{2\rho_t^2}{w_0^2}\right) e^{-\left(\frac{\rho_t^2}{w_0^2}\right)} e^{-il\varphi}\ e^{ikz} \hat{e_x} \tag{9}$$

$$\hat{e_x} = sin\theta\ cos\varphi\ \hat{e_r} + cos\theta\ cos\varphi\ \ \hat{e_\theta} - sin\varphi\ \ \hat{e_\phi} \tag{10}$$

where $\hat{e_x}$ stands for the polarization unit vector in the spherical coordinates system. $L_p^l(.)$ be the associated Legendre polynomial. It is given as,

$$L_p^l\left(\frac{2\rho^2}{w_0^2}\right) = \sum_{m=0}^{p} \frac{(-1)^m (p+l)!}{(p-m)!m!(l+m)!} \left(\frac{2\rho^2}{w_0^2}\right)^m \tag{11}$$

Here, p and l are the radial and azimuthal modes. Where, $\rho_t = \rho\ cos\theta\ (0 \le \theta \le \pi)$ be the cylindrical transverse coordinate. We focused to study the scattering characteristics of PEMC sphere with dimensions significantly smaller than the beam waist radius, so, we use a value near the optical axis to approximate the incident field i.e., $(\rho_t \ll a)$. The incident field for zeroth radial i.e., $(p = 0)$ and l^{th} order angular LG mode modified as,

$$\vec{E}^{inc} = E_0 \left(\frac{\rho_t \sqrt{2}}{w_0}\right)^l e^{i(kz - l\varphi)} (sin\theta\ cos\varphi\ \hat{e_r} + cos\theta\ cos\varphi\ \ \hat{e_\theta} - sin\varphi\ \ \hat{e_\phi}) \tag{12}$$

The incident EM fields for LG vortex EM wave using SVWF's can be given as (Bohren and Huffman, 2008),

$$\vec{E}^{inc} = \sum_{m=l\pm1}^{\infty} \sum_{n=m}^{\infty} (B_{emn}^i \vec{M}_{emn}^{(1)} + B_{omn}^i \vec{M}_{omn}^{(1)} + A_{emn}^i \vec{N}_{emn}^{(1)} + A_{omn}^i \vec{N}_{omn}^{(1)}) \tag{13}$$

$$\vec{H}^{inc} = -\left(\frac{k_0}{\omega \mu_0}\right) \sum_{m=l\pm1}^{\infty} \sum_{n=m}^{\infty} (B_{emn}^i \vec{N}_{emn}^{(1)} + B_{omn}^i \vec{N}_{omn}^{(1)} + A_{emn}^i \vec{M}_{emn}^{(1)} + A_{omn}^i \vec{M}_{omn}^{(1)}) \tag{14}$$

For m parameter, the selection rules in the field's expression for VEM wave are designated as,

$$m = \begin{cases} 1 & l = 0\ (Plane\ wave) \\ l \pm 1 & l \neq 0\ (VEM\ wave) \end{cases} \tag{15}$$

The scattered electric and magnetic fields for VEM wave can be expanded as,

$$\vec{E}^{sca} = \sum_{m=l\pm1}^{\infty} \sum_{n=m}^{\infty} (b^s_{emn}\vec{M}^{(3)}_{emn} + b^s_{omn}\vec{M}^{(3)}_{omn} + a^s_{emn}\vec{N}^{(3)}_{emn} + a^s_{omn}\vec{N}^{(3)}_{omn}) \tag{16}$$

$$\vec{H}^{sca} = -(\frac{k_0}{\omega\mu_0}) \sum_{m=l\pm1}^{\infty} \sum_{n=m}^{\infty} (b^s_{emn}\vec{N}^{(3)}_{emn} + b^s_{omn}\vec{N}^{(3)}_{omn} + a^s_{emn}\vec{M}^{(3)}_{emn} + a^s_{omn}\vec{M}^{(3)}_{omn}) \tag{17}$$

Here, k_0 and μ_0 represent wave number phase constant and permeability for the free space. Where, $B^i_{emn}, B^i_{omn}, A^i_{emn},\ and\ A^i_{omn}$ represent the unknown expansion coefficients. These coefficients can be found with mathematical steps toward the VEM wave as,

$$B^i_{emn} = \frac{\int_0^{2\pi}\int_0^{\pi} \vec{E}^{inc}.\ \vec{M}_{emn}\ sin\theta\ d\theta d\varphi}{\int_0^{2\pi}\int_0^{\pi} |\vec{M}_{emn}|^2\ sin\theta\ d\theta d\varphi} \tag{18}$$

and

$$B^i_{omn} = \frac{\int_0^{2\pi}\int_0^{\pi} \vec{E}^{inc}.\ \vec{M}_{omn}\ sin\theta\ d\theta d\varphi}{\int_0^{2\pi}\int_0^{\pi} |\vec{M}_{omn}|^2\ sin\theta\ d\theta d\varphi} \tag{19}$$

Similarly, $A^i_{emn}\ and\ A^i_{omn}$ can be determined.

The boundary conditions for radial EM field components is

$$\epsilon_0 E^{inc}_r + \epsilon_0 E^{sca}_r - M\mu_0 H^{inc}_r - M\mu_0 H^{sca}_r = 0 \tag{20}$$

and the boundary conditions for tangential EM field components is

$$H^{inc}_t + ME^{inc}_t + H^{sca}_t + ME^{sca}_t = 0 \tag{21}$$

On implementing the above boundary conditions, the (radial + tangential) field components on the surface of the PEMC sphere becomes zero i.e., $r = a$ (Ruppin, 2006).

Then, scattering coefficients in connection with the incident field coefficients for VEM wave after a cumbersome work become as,

$$a^s_{omn} = -A^i_{omn} \frac{(h_n(\rho)[\rho h_n(\rho)]' + M^2\eta_0^2 h_n(\rho)[\rho j_n(\rho)]')}{h_n(\rho)[\rho h_n(\rho)]'(1+M^2\eta_0^2)} - iM\eta_0 B^i_{omn} \frac{(j_n(\rho)[\rho h_n(\rho)]' - h_n(\rho)[\rho j_n(\rho)]')}{h_n(\rho)[\rho h_n(\rho)]'(1+M^2\eta_0^2)} \tag{22}$$

$$b^s_{omn} = -B^i_{omn} \frac{(h_n(\rho)[\rho j_n(\rho)]' + M^2\eta_0^2 j_n(\rho)[\rho h_n(\rho)]')}{h_n(\rho)[\rho h_n(\rho)]'(1+M^2\eta_0^2)} - iM\eta_0 A^i_{omn} \frac{(h_n(\rho)[\rho j_n(\rho)]' - h_n(\rho)[\rho h_n(\rho)]')}{h_n(\rho)[\rho h_n(\rho)]'(1+M^2\eta_0^2)} \tag{23}$$

$$a^s_{emn} = -A^i_{emn} \frac{(j_n(\rho)[\rho h_n(\rho)]' + M^2\eta_0^2 h_n(\rho)[\rho j_n(\rho)]')}{h_n(\rho)[\rho h_n(\rho)]'(1+M^2\eta_0^2)} - iM\eta_0 B^i_{emn} \frac{(j_n(\rho)[\rho h_n(\rho)]' - h_n(\rho)[\rho j_n(\rho)]')}{h_n(\rho)[\rho h_n(\rho)]'(1+M^2\eta_0^2)} \tag{24}$$

$$b^s_{emn} = -B^i_{emn} \frac{(h_n(\rho)[\rho j_n(\rho)]' + M^2\eta_0^2 j_n(\rho)[\rho h_n(\rho)]')}{h_n(\rho)[\rho h_n(\rho)]'(1+M^2\eta_0^2)} - iM\eta_0 A^i_{emn} \frac{(h_n(\rho)[\rho j_n(\rho)]' - j_n(\rho)[\rho h_n(\rho)]')}{h_n(\rho)[\rho h_n(\rho)]'(1+M^2\eta_0^2)} \tag{25}$$

As, this research deals with the use of SVWF's to calculate the scattered field by a PEMC sphere when the topological charge/OAM mode number i.e., $(l = 1)$. So, using the selection rule for LG VEM wave $(l = 1)$ and maximum $n = 2$ using equation (15), the incidence electric field expansion can be given as,

$$\vec{E}^{inc} = B^i_{e00}M^{(1)}_{e00} + B^i_{o00}M^{(1)}_{o00} + A^i_{e00}N^{(1)}_{e00} + A^i_{o00}N^{(1)}_{00} + B^i_{e01}M^{(1)}_{e01} + B^i_{o01}M^{(1)}_{o01} + A^i_{e01}N^{(1)}_{e01} + A^i_{o01}N^{(1)}_{o01} + B^i_{e11}M^{(1)}_{e11} + B^i_{o11}M^{(1)}_{o11} + A^i_{e11}N^{(1)}_{e11} + A^i_{o11}N^{(1)}_{o11} + B^i_{e02}M^{(1)}_{e02} + B^i_{o02}M^{(1)}_{o02} + A^i_{e02}N^{(1)}_{e02} + A^i_{o02}N^{(1)}_{o02} + B^i_{e12}M^{(1)}_{e12} + B^i_{o12}M^{(1)}_{o12} + A^i_{e12}N^{(1)}_{e12} + A^i_{o12}N^{(1)}_{o12} + B^i_{e22}M^{(1)}_{e22} + B^i_{o22}M^{(1)}_{o22} + A^i_{e22}N^{(1)}_{e22} + A^i_{o22}N^{(1)}_{o22} \quad (26)$$

Here, we only consider the terms with $(m = 0, 2)$. The incident field coefficients as, $B_{o00}, A_{o00}, B_{o01}, A_{o01}, B_{o02}, A_{o02}, B_{e00}, A_{e00}$ vanish and $B_{e11}, B_{o11}, A_{e11}, A_{o11}, B_{e12}, B_{o12}$ are excluded. So, the incident and scattered field expressions can be modified as,

$$\vec{E}^{inc} = B^i_{e01}M^{(1)}_{e01} + B^i_{e02}M^{(1)}_{e02} + A^i_{e02}N^{(1)}_{e02} + B^i_{e22}M^{(1)}_{e22} + B^i_{o22}M^{(1)}_{o22} + A^i_{e22}N^{(1)}_{e22} + A^i_{o22}N^{(1)}_{o22} \quad (27)$$

$$\vec{E}^{sca} = b^s_{e01}M^{(3)}_{e01} + b^s_{e02}M^{(3)}_{e02} + a^s_{e02}N^{(3)}_{e02} + b^s_{e22}M^{(3)}_{e22} + b^s_{o22}M^{(3)}_{o22} + a^s_{e22}N^{(3)}_{e22} + a^s_{o22}N^{(3)}_{o22} \quad (28)$$

4. Optical radiation force (F_z)

It is very known fact that light associates with momentum in addition to energy. Hence, the interaction of a photon with the material particle, the exchange of energy and momentum occurs, so leads to the optical radiation force (RF). In electrodynamics (Bohren and Huffman, 2008; Jackson, 1999), the expression for the time averaged force is given as,

$$< F >= -\left(\frac{1}{2c}\right)\epsilon_0\eta_0 Re\int_0^{2\pi}\int_0^{\pi}[\boldsymbol{E}^{tot} \times \boldsymbol{H}^{tot*}]\, r^2 sin\theta\, d\theta d\varphi \quad (29)$$

The operator < > be the time average. In above, superscript "tot" represents the imposition of the incident and scattered EM fields i.e.,

$$\boldsymbol{E}^{tot} = \vec{E}^{inc} + \vec{E}^{sca} \quad (30)$$

$$\boldsymbol{H}^{tot} = \vec{H}^{inc} + \vec{H}^{sca} \quad (31)$$

The substitution of the incident and scattered EM fields into equation (29), yields the RF after rigorous calculation as,

$$F_z = \left(\frac{-2}{\rho^2}\right)\left(\frac{\sqrt{2}E_0}{\pi\, c\, w_0^2\, k_0^2}\right) Re\sum_{m=l\pm1}^{\infty}\sum_{n=m}^{\infty}\left\{\frac{n(n+2)}{n+1}[(a^s_{omn} + b^s_{omn} + a^s_{omn+1} + b^s_{omn+1}) + 2(a^s_{omn}a^{s*}_{omn+1} + b^s_{omn}b^{s*}_{omn+1} + a^s_{emn}a^{s*}_{emn+1} + b^s_{emn}b^{s*}_{emn+1})] + \frac{2n+1}{n(n+1)}\,(a^s_{omn} + b^s_{omn} + 2a^s_{omn}b^{s*}_{omn} + 2a^s_{emn}b^{s*}_{emn})\right\} \quad (32)$$

As PEMC sphere is centered on the z-axis of VEM wave propagation so, the transverse RF components i.e., $F_x = F_y = 0$.

The terms in the curly brackets are called RF efficiency for VEM wave and denoted by Q_{oam}. It can be decomposed into sum of two Q factors as,

$$Q_{oam}^{tot} = Q_{oam}^{\parallel} + Q_{oam}^{\perp} \tag{33}$$

Here,

$$Q_{oam}^{\parallel} = \left(\frac{-2}{\rho^2}\right)\left(\frac{\sqrt{2}E_0}{w_0\, k_0}\right) Re \sum_{m=l\pm1}^{\infty} \sum_{n=m}^{\infty} \left\{\frac{n(n+2)}{n+1}[(a_{omn}^{s} + b_{omn}^{s} + a_{omn+1}^{s} + b_{omn+1}^{s}) + 2(a_{omn}^{s} a_{omn+1}^{s*} + b_{omn}^{s} b_{omn+1}^{s*})] + \frac{2n+1}{n(n+1)}\,(a_{omn}^{s} + b_{omn}^{s} + 2a_{omn}^{s} b_{omn}^{s*})\right\} \tag{34}$$

and,

$$Q_{oam}^{\perp} = \left(\frac{-4}{\rho^2}\right)\left(\frac{\sqrt{2}E_0}{w_0\, k_0}\right) Re \sum_{m=l\pm1}^{\infty} \sum_{n=m}^{\infty} \left\{\frac{n(n+2)}{n+1}[(a_{emn}^{s} a_{emn+1}^{s*} + b_{emn}^{s} b_{emn+1}^{s*})] + \frac{2n+1}{n(n+1)}\,(a_{emn}^{s} b_{emn}^{s*})\right\} \tag{35}$$

These factors are somewhat different from standard mathematical expressions of plane wave (absence of field modes) which are given in (Bohren and Huffman, 2008), as multiple internal field modes are involved for VEM wave.

5. Cross-section factors calculations

To examine the interaction of VEM wave with the PEMC sphere, the Q factors are computed and presented. The Q_{sca}, Q_{abs}, and Q_{ext} are determined using the following expressions as given in (Bohren and Huffman, 2008; Ruppin, 2006) on integrating over a PEMC sphere for VEM wave. The expressions for these are given as,

$$Q_{ext} = \left(\frac{-2}{\rho^2}\right) Re \sum_{m=l\pm1}^{\infty} \sum_{n=m}^{\infty} (2n+1)(a_{omn}^{s} + b_{omn}^{s}) \tag{36}$$

$$Q_{sca} = \left(\frac{2}{\rho^2}\right) \sum_{m=l\pm1}^{\infty} \sum_{n=m}^{\infty} (2n+1)(|a_{omn}^{s}|^2 + |b_{omn}^{s}|^2 + |a_{emn}^{s}|^2 + |b_{emn}^{s}|^2) \tag{37}$$

The Q_{ext} in literature (Bohren and Huffman, 2008; Jackson, 1999) is taken as sum of two Q factors i.e., Q_{sca} and Q_{abs} as,

$$Q_{ext} = Q_{abs} + Q_{sca} \tag{38}$$

As the PEMC sphere is totally reflecting so, Q_{abs} becomes zero. Therefore, the extinction cross section becomes equal to the scattering cross section i.e., $Q_{ext} = Q_{sca}$. No loss occurs inside it (energy conservation principle). Hence, the equation (38) dictates that for the PEMC sphere, Q_{sca} has equal contribution to that of Q_{ext}.

6. Numerical validation

Furthermore, to check the validity of the numerical codes, the Q_{sca} parameter of PEMC sphere as function of scattering angle is compared under special condition i.e., $l = 0$. It is observed that Q_{sca}

of plane wave exerted on PEMC sphere as given in equation (21) of (Ruppin, 2006), agrees very well with our present work on making ($l = 0$). This confirms the accuracy of our analytical theory and computation. The graphical analysis is shown in Figure 2.

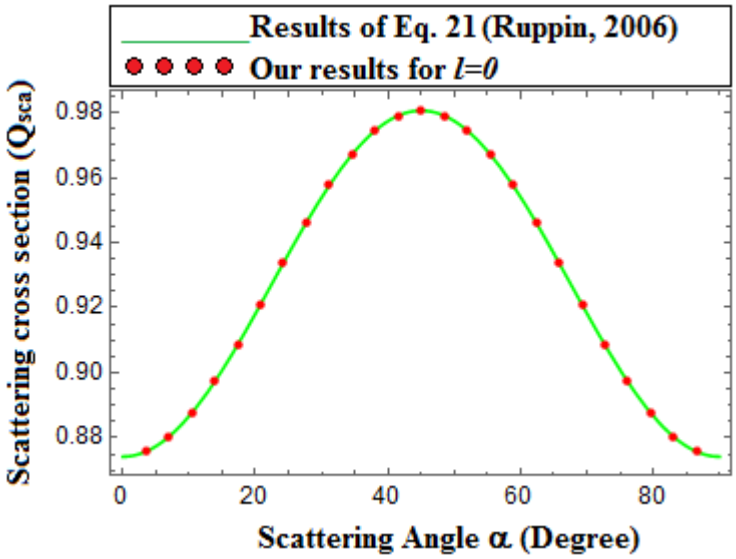

Fig. 2. Comparison of present research for scattering cross-section (Q_{sca}) of PEMC sphere vs. scattering angle (α°) for ($l = 0$) i.e., no OAM and results of equation (21) of published work (Ruppin, 2006).

7. Results and Discussions

The equations (22)-(25) contribute the final results towards optical RF in the longitudinal direction i.e., along direction of wave propagation for the PEMC sphere. Both the field coefficients as, co- and cross-polarized for the PEMC sphere contribute equally. The scattering coefficients in equations (22)-(25) for VEM wave scattering through the PEMC sphere depend on the value of admittance parameter M, that characterize the sphere material. The scattered field distribution changes on changing the parameter M. To study the PEMC characteristics, parameter M with infinite range extension is defined as (Ruppin, 2006),

$$M\eta_0 = \tan\alpha \tag{39}$$

On making ($\alpha = 0^{\circ}, 90^{\circ} \rightarrow M\eta_0 = 0, \infty$), the PEMC converted into PMC and PEC respectively. In between 0° and 90°, the characteristics for PEMC medium can be seen. As we interested to study the Q_{sca} parameter to exploit the scattering information so, the Q_{sca} would be more focused on ward to analyze the interaction of VEM wave with PEMC sphere.

Figure 3 shows the influence of the sphere size parameter (ρ) on Q_{sca} of PEMC sphere. Firstly, a large shift can be seen and the maximum scattering decrease is observed. The absolute value of the Q_{sca} becomes much smaller for the OAM wave since the intensity shifts to zero away from the optical axis. The results show difference in the graph toward VEM wave; the reason behind this phenomenon is, internal field modes are involved in the scattering of VEM wave,

which are different from plane wave scattering (i.e., ($l = 0$) no OAM). On increasing ρ, the Q_{sca} decreases.

Figure 3 also displays with the increase of ρ parameter, the width of Q_{sca} decreases. The Q_{sca} depicts non stability in magnitude and change able behavior, however after $\alpha = 40^0$, the Q_{sca} reduces and meets zero, indicating that the minimal scattering happened. As the scattered field intensity approaches zero farther from the optical axis, the Q_{sca} for VEM wave decreases.

The effects of beam waist radius (w_0) on the Q_{sca} are considered in Figure 4. It shows that changing w_0, from 0.1 λ, 0.2 λ, and 0.3 λ, the Q_{sca} decreases sequentially and then drop to zero. A small changing in the w_0, a large decrease for Q_{sca} can be seen. The Q_{sca} is significantly affected by variations in w_0. The change of the $M\eta_0$ parameter has a clear influence on the Q_{sca}, as seen in Figure 5.

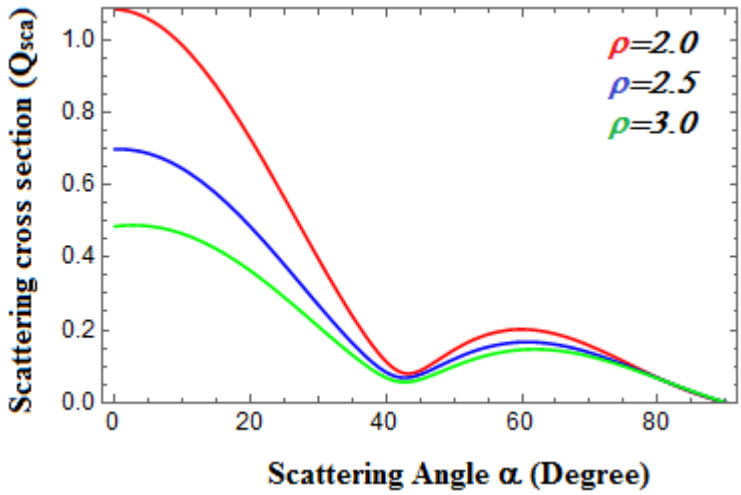

Fig. 3. Influence of sphere size parameter (ρ) on the scattering cross-section (Q_{sca}) for OAM wave exerted on PEMC sphere.

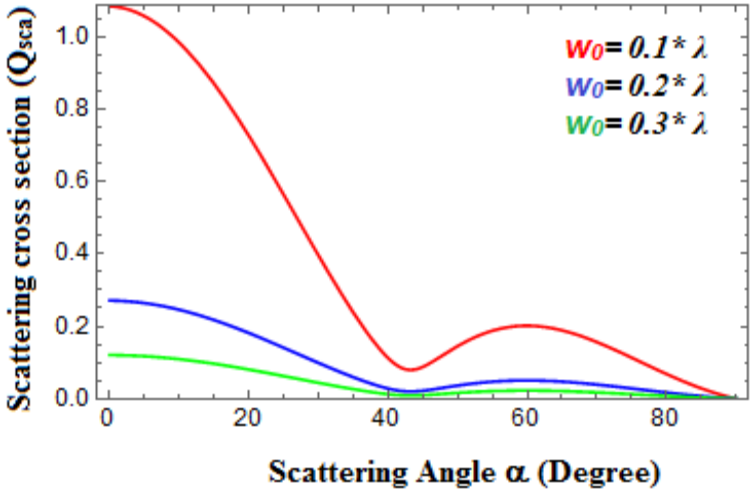

Fig. 4. Influence of beam waist radius (w_0) on the scattering cross section (Q_{sca}) for OAM wave exerted on PEMC sphere.

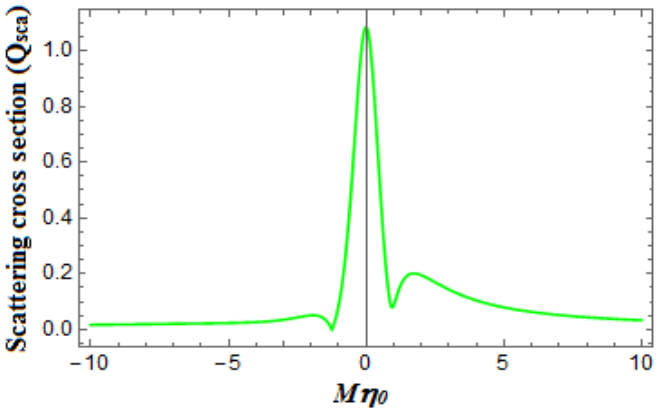

Fig. 5. Influence of $M\eta_0$ on the scattering cross-section (Q_{sca}) for OAM wave exerted on PEMC sphere.

The Q_{sca} shows flat response away from the optical center but around the center where ($M\eta_0 = 0$), it begins to rise, then peaks, and then gradually declines. This is due to the fact that specific OAM field modes are included around the center of the optical axis for $M\eta_0 = 0$. Farther from the optical axis center, the lack of field modes is observed. Figure 6 shows that the optical RF vary with ρ parameter. It can be summed up from Figure 6, with the increase of ρ, the RF distribution increases. So, it is referred from Figure 6, varying ρ had slight effect on RF. However, as ρ increases, optical RF reaches linearly up to a maximum at $\alpha = 55^0$, and then decays for remaining values of scattering angle. The RF shows symmetric behavior versus scattering angle i.e., $\alpha = 0^0 - 90^0$, while from $90^0 - 180^0$, this behavior changes.

Fig. 7 shows that the optical RF vary with the waist radius (w_0). The plots in Figure 7 depict that RF is more sensitive by changing values of w_0. Furthermore, with the increase of w_0, the amplitude of the distribution of the optical RF increases. Besides, a continuous increase in w_0, a remarkable change for the RF can be observed. So, the scattering force contributes toward thrusting the particle. Figure 7 graphical results also explain that with the increase of w_0, the width of RF becomes narrow.

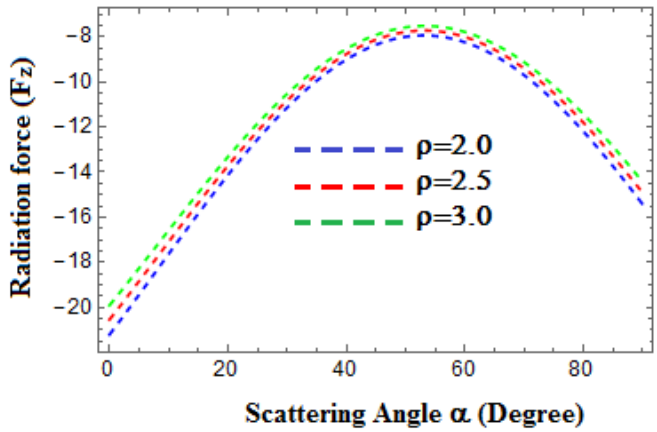

Fig. 6. Influence of sphere size parameter (ρ) on the radiation force (F_z) for OAM wave exerted on PEMC sphere.

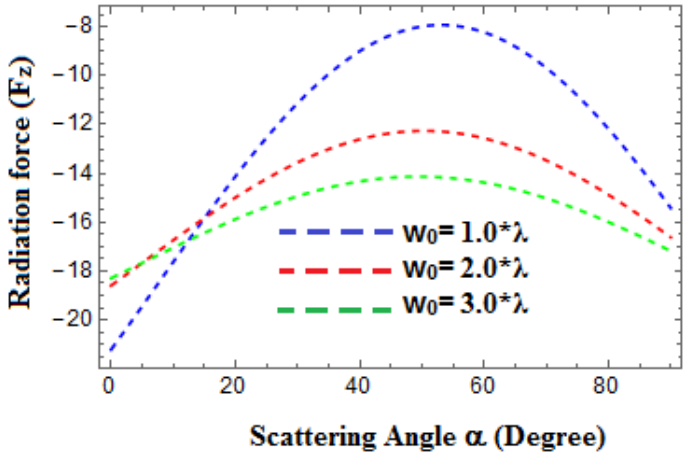

Fig. 7. Influence of beam waist radius (w_0) on the radiation force (F_z) for OAM wave exerted on PEMC sphere.

Figure 8 displays the plot for the optical RF for w_0 versus $M\eta_0$ parameter. Due to the helical distribution of OAM wave intensity, the optical RF has some specific peak values. The increase of w_0 against $M\eta_0$ parameter, the RF extends a large distance from the optical axis. However, a fine symmetry is to be seen. With the increase of w_0, the width of RF decreases. This happens due to extension of the OAM wave intensity distribution. As the particles deviate from the optical axis of the PEMC sphere, they feel a pushing force aside from the OAM axis.

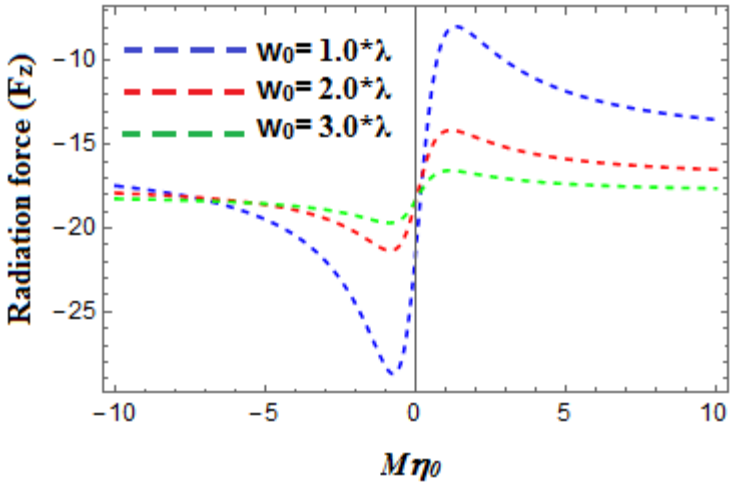

Fig. 8. Influence of beam waist radius (w_0) on the radiation force (F_z) versus $M\eta_0$ parameter for OAM wave exerted on PEMC sphere.

8. Conclusions

In this analysis, a theoretical formalism to study the scattering cross-section (Q_{sca}) along with EM radiation force (RF) for VEM wave exerted on a PEMC sphere is developed. The Q_{sca} and optical RF can be modulated by changing the sphere size parameter, beam waist radius, and $M\eta_0$ parameter. The response of RF is found to be very little for sphere size parameter in-contrast to

beam waist radius. However, the response of RF and Q_{sca} is observed to be the same for beam waist radius i.e., on increasing the waist radius, both factors decrease. As compared to plane wave scattering, internal field modes are involved for VEM wave interaction towards the PEMC sphere; so, this became clearer to see the effective response towards the Q_{sca} and RF. This investigation provides comprehensive detail about RF and Q_{sca} for VEM wave as compared to the plane wave. The scope of this study can be expanded to study the interaction of LG VEM wave for metamaterial structures.

Financial and Ethical disclosures

The authors have no conflict of interest.

ACKNOWLEDGMENTS

The authors extend their appreciation to the Deputyship for Research and Innovation, "Ministry of Education" in Saudi Arabia for funding this research work through the project number IFKSURG-2-676.

References

Achard, F. (2005). James Clerk Maxwell, A Treatise On Electricity And Magnetism, (1873). Landmark Writings In Western Mathematics. Elsevier. 1640-1940.

Allen, L., Beijersbergen, M. W., Spreeuw, R. & Woerdman, J. (1992). Orbital Angular Momentum Of Light And The Transformation Of Laguerre-Gaussian Laser Modes. Physical Review A, 45**,** 8185-8189.

Arfan, M., Alkanhal, M. A., Ghaffar, A. & Alqahtani, A. H. (2022a). Scattering Of Laguerre–Gaussian Beam From A Chiral-Coated Perfect Electromagnetic Conductor (PEMC) Cylinder. Journal Of Computational Electronics**,** 1-10.

Arfan, M., Ghaffar, A., Alkanhal, M. A., Naz, M., Alqahtani, A. H. & Khan, Y. (2022b). Orbital Angular Momentum Wave Scattering From Perfect Electromagnetic Conductor (PEMC) Sphere. Optik**,** 168562.

Arfan, M., Ghaffar, A., Naz, M. & Hanif, M. (2021). Radar Cross Section (RCS) Of Perfect Electromagnetic Conductor (PEMC) Cylinder By A Laguerre–Gaussian Beam. Kuwait Journal Of Science.

Azarpeyvand, M. & Azarpeyvand, M. (2013). Acoustic Radiation Force On A Rigid Cylinder In A Focused Gaussian Beam. Journal Of Sound And Vibration, 332**,** 2338-2349.

Barnett, S. M. & Allen, L. (1994). Orbital Angular Momentum And Nonparaxial Light Beams. Optics Communications, 110**,** 670-678.

Bohren, C. F. & Huffman, D. R. (2008). Absorption And Scattering Of Light By Small Particles, John Wiley & Sons.

Capolino, F. (2017). Theory And Phenomena Of Metamaterials, Crc Press.

Cheng, W., Zhang, W., Jing, H., Gao, S. & Zhang, H. (2018). Orbital Angular Momentum For Wireless Communications. Ieee Wireless Communications, 26**,** 100-107.

Gibson, G., Courtial, J., Padgett, M. J., Vasnetsov, M., Pas'ko, V., Barnett, S. M. & Franke-Arnold, S. (2004). Free-Space Information Transfer Using Light Beams Carrying Orbital Angular Momentum. Optics Express, 12**,** 5448-5456.

Jackson, J. D. (1999). Classical Electrodynamics. American Association Of Physics Teachers.

Kim, J. S. & Lee, S. S. (1983). Scattering Of Laser Beams And The Optical Potential Well For A Homogeneous Sphere. Josa, 73**,** 303-312.

Kim, S. B. & Kim, S. S. (2006). Radiation Forces On Spheres In Loosely Focused Gaussian Beam: Ray-Optics Regime. Josa B, 23**,** 897-903.

Kiselev, A. D. & Plutenko, D. O. (2016). Optical Trapping By Laguerre-Gaussian Beams: Far-Field Matching, Equilibria, And Dynamics. Physical Review A, 94**,** 013804.

Kotlyar, V. & Nalimov, A. (2006). Analytical Expression For Radiation Forces On A Dielectric Cylinder Illuminated By A Cylindrical Gaussian Beam. Optics Express, 14**,** 6316-6321.

Lapine, M. & Tretyakov, S. (2007). Contemporary Notes On Metamaterials. Iet Microwaves, Antennas & Propagation, 1**,** 3-11.

Lebedev, P. (1883). Experimental Examination Of Light Pressure. Nuovo Cimento, 15**,** 195.

Li, Y., Zhou, L.-M. & Zhao, N. (2021). Anomalous Motion Of A Particle Levitated By Laguerre–Gaussian Beams. Optics Letters, 46**,** 106-109.

Li, Z.-J., Wu, Z.-S. & Shang, Q.-C. (2011). Calculation Of Radiation Forces Exerted On A Uniaxial Anisotropic Sphere By An Off-Axis Incident Gaussian Beam. Optics Express, 19**,** 16044-16057.

Liu, K., Gao, Y., Li, X. & Cheng, Y. (2018). Target Scattering Characteristics For Oam-Based Radar. Aip Advances, 8**,** 0250021-0250033.

Long, L., Hao, X. & Qiang, F. (2018). Research Progresses In Theory And Applications Of Vortex Electromagnetic Waves. Journal Of Microwaves, 34**,** 1-12.

Mitri, F. (2016). Acoustic Backscattering And Radiation Force On A Rigid Elliptical Cylinder In Plane Progressive Waves. Ultrasonics, 66**,** 27-33.

Mitri, F. (2018). Electromagnetic Binding And Radiation Force Reversal On A Pair Of Electrically Conducting Cylinders Of Arbitrary Geometrical Cross-Section With Smooth And Corrugated Surfaces. Osa Continuum, 1**,** 521-541.

Mitri, F. (2019a). Electromagnetic Radiation Force On A Perfect Electromagnetic Conductor (Pemc) Circular Cylinder. Journal Of Quantitative Spectroscopy And Radiative Transfer, 233**,** 21-28.

Mitri, F. (2019b). Induced Radiation Force Of An Optical Line Source On A Cylinder Material Exhibiting Circular Dichroism. Josa A, 36**,** 1648-1656.

Mitri, F. (2019c). Optical Radiation Force Expression For A Cylinder Exhibiting Rotary Polarization In Plane Quasi-Standing, Standing, Or Progressive Waves. Josa A, 36**,** 768-774.

Mitri, F., Li, R. & Sun, H. (2020). Optical Radiation Force On A Perfect Electromagnetic Conductor (Pemc) Sphere. Journal Of Quantitative Spectroscopy And Radiative Transfer, 256**,** 107280.

Molina-Terriza, G., Torres, J. P. & Torner, L. (2007). Twisted Photons. Nature Physics, 3**,** 305-310.

Nichols, E. F. & Hull, G. F. (1903). The Pressure Due To Radiation.(Second Paper.). Physical Review (Series I), 17**,** 26.

O'neil, A., Macvicar, I., Allen, L. & Padgett, M. (2002). Intrinsic And Extrinsic Nature Of The Orbital Angular Momentum Of A Light Beam. Physical Review Letters, 88**,** 053601.

Olsen, H., Romberg, W. & Wergeland, H. (1958). Radiation Force On Bodies In A Sound Field. The Journal Of The Acoustical Society Of America, 30**,** 69-76.

Padgett, M. (2014). Light's Twist. Proceedings Of The Royal Society A: Mathematical, Physical And Engineering Sciences, 470**,** 20140633.

Qu, T., Wu, J., Wu, Z., Shang, Q. & Li, Z. (2016). Scattering Of A Uniaxial Anisotropic Sphere Incident By A Laguerre-Gaussian Vortex Beam. 11th International Symposium On Antennas, Propagation And Em Theory (Isape). IEEE, 557-560.

Qu, T., Wu, Z.-S., Shang, Q.-C. & Li, Z.-J. (2016b). Light Scattering Of A Laguerre–Gaussian Vortex Beam By A Chiral Sphere. Josa A, 33**,** 475-482.

Qu, T., Wu, Z.-S., Shang, Q.-C., Li, Z.-J., Bai, L. & Gong, L. (2015). Analysis Of The Radiation Force Of A Laguerre Gaussian Vortex Beam Exerted On An Uniaxial Anisotropic Sphere. Journal Of Quantitative Spectroscopy And Radiative Transfer, 162**,** 103-113.

Qu, T., Wu, Z., Shang, Q., Li, Z., Wu, J. & Li, H. (2018). Scattering And Propagation Of A Laguerre–Gaussian Vortex Beam By Uniaxial Anisotropic Bispheres. Journal Of Quantitative Spectroscopy And Radiative Transfer, 209**,** 1-9.

Ruppin, R. (2006). Scattering Of Electromagnetic Radiation By A Perfect Electromagnetic Conductor Sphere. Journal Of Electromagnetic Waves And Applications, 20**,** 1569-1576.

Shahid, M. U., Ghaffar, A., Alkanhal, M. A. & Khan, Y. (2021). Propagation Of Electromagnetic Waves In Graphene-Wrapped Cylindrical Waveguides Filled With Magnetized Plasma. Optik, 244**,** 167566.

Sihvola, A. (2007). Metamaterials In Electromagnetics. Metamaterials, 1**,** 2-11.

Sihvola, A. & Lindell, I. V. 2017. Bianisotropic Materials And Pemc. *Theory And Phenomena Of Metamaterials.* Crc Press.

Simpson, N., Allen, L. & Padgett, M. (1996). Optical Tweezers And Optical Spanners With Laguerre–Gaussian Modes. Journal Of Modern Optics, 43**,** 2485-2491.

Thakur, A. & Berakdar, J. (2012). Reflection And Transmission Of Twisted Light At Phase Conjugating Interfaces. Optics Express, 20**,** 1301-1307.

Thidé, B., Then, H., Sjöholm, J., Palmer, K., Bergman, J., Carozzi, T., Istomin, Y. N., Ibragimov, N. & Khamitova, R. (2007). Utilization Of Photon Orbital Angular Momentum In The Low-Frequency Radio Domain. Physical Review Letters, 99**,** 087701.

Wartak, M. S., Tsakmakidis, K. L. & Hess, O. (2011). Introduction To Metamaterials. Physics In Canada, 67**,** 30-34.

Yao, A. M. & Padgett, M. J. (2011). Orbital Angular Momentum: Origins, Behavior And Applications. Advances In Optics And Photonics, 3**,** 161-204.

Yao, Y., Liang, X., Zhu, M., Zhu, W., Geng, J. & Jin, R. (2019). Analysis And Experiments On Reflection And Refraction Of Orbital Angular Momentum Waves. Ieee Transactions On Antennas And Propagation, 67**,** 2085-2094.

Yu, H. & She, W. (2015). Radiation Force Exerted On A Sphere By Focused Laguerre–Gaussian Beams. Josa A, 32**,** 130-142.

Submitted: 02/06/2022
Revised: 24/06/2022
Accepted: 27/06/2022
DOI: 10.48129/kjs.20775